Redirecting on-surface cycloaddition reactions in a self-assembled ordered molecular array on graphite

Yu Li Huang,*[1,6] Ke Yang,[2,6] Jing Yang,[3,6] Sisheng Duan,[4] Yihe Wang,[1,5] Mingyue Sun,[1,4] Yong-Wei Zhang,*[2] Ming Yang,*[2] and Andrew T. S. Wee[4]

[1]Joint School of National University of Singapore and Tianjin University, International Campus of Tianjin University, Binhai New City, Fuzhou, 350207, China

[2]Department of Applied Physics, The Hong Kong Polytechnic University, Kowloon, Hong Kong SAR, China

[3]Institute of High Performance Computing (IHPC), Agency for Science, Technology and Research (A*STAR), 1 Fusionopolis Way, #16-16 Connexis, Singapore 138632, Republic of Singapore

[4]Department of Physics, National University of Singapore, Singapore 117542, Singapore

[5]Department of Chemistry, National University of Singapore, Singapore 117543, Singapore

[6]These authors contributed equally to this work.

*Corresponding Authors: hyl@tjufz.org.cn, zhangyw@ihpc.a-star.edu.sg, kevin.m.yang@polyu.edu.hk

Abstract

The synthesis of atomically precise carbon nanostructures in ultra-high vacuum has seen extensive progress on metal surfaces. However, this remains challenging on chemically inert surfaces. It is because the thermally activated C-C coupling encounters a severe "desorption problem" on weakly interacting substrates. In this study, we report an extraordinary [2+2+2+2] cycloaddition occurred in a highly ordered π-conjugated molecular array on graphite, via Fe-mediated dehydrohalogenative reactions using scanning tunneling microscopy. This is in contrast to the dehalogenative [2+2] cycloaddition reactions previously reported on noble metal surface. More interestingly, various products are observed and embedded in the close-packing supramolecular arrays as defective individuals or chains (grain boundaries). First-principles calculations reveal that the energy barriers of the multiple dehalogenation, dehydrogenation, and cycloaddition reactions are reduced by catalytic Fe atoms but

remain energetically unfavorable. As thus, additional intermolecular coupling, steric hindrance, and/or interfacial interactions could play significant roles on redirecting the reaction processes. This study introduces a new paradigm for understanding on-surface synthesis on non-metal substrates.

Introduction

On-surface synthesis in ultrahigh vacuum (UHV) has garnered intensive interest as a promising approach to fabricate atomically precise organic nanostructures with tunable functionality.[1-3] In particular, surface-assisted dehalogenative and/or dehydrogenative cycloaddition reactions, stemming from the conventional Ullmann coupling, have predominantly been showcased on noble metal surfaces. These reactions have generated a variety of complex π-conjugated structures, including nanographenes,[4-6] carbon nanoribbons,[7, 8] and others.[9] It is well understood that the metal substrates not only serve as a surface for hosting the precursors, intermediates, and final products, but also provide metal catalytic agents for the reactions and even constituents of organometallic intermediates.[10-12] Thus, the reaction pathways, activation barriers, and product outcomes may vary significantly on different metal surfaces using the same precursor.[11, 13] Furthermore, metal substrates could strongly screen the intrinsic properties of the designed nanostructures and might limit their applications.[14-18]

Much work has also been devoted to the on-surfaces synthesis on non-metal substrates.[17, 19-21] Various strategies have been developed to facilitate chemical reactions on substrates such as rutile TiO_2,[22, 23] calcite $CaCO_3$,[24] mica,[25] NaCl,[26, 27] and even single-layered graphene[28] and boron nitride (BN)[29] on metal surfaces, assisted by pre-designed precursors, guest catalytic agents, photocatalysis, or tip manipulations under vacuum conditions. In particular, chemically inert graphite has been widely used in traditional in-solution synthesis of two-dimensional (2D) covalent organic frameworks via reversible condensation reactions,[19, 30-34] as well as mesoscale photopolymerization in UHV.[35] Graphite is also highly desirable for precisely characterizing the intrinsic properties of on-surface synthesized nanostructures, benefiting from its atomical flatness and electronic decoupling. However, thermally activated C-C recombination in UHV remains elusive on such an inert substrate due to the "desorption problem".[19] This arises when the reactants prematurely desorb from the surface before the reaction can occur, which depends on the delicate balance between the reaction barrier and the

desorption threshold. Moreover, the underlying reaction mechanism on such chemically inert surface may distinctly differ from the extensively studied metal surfaces, presenting opportunities for further investigation.

Here we present the realization of Fe-assisted cycloaddition reactions in a close-packed, highly ordered supramolecular array assembled on graphite surface via mild annealing. 2,3,6,7,10,11-hexabromotriphenylene (HBTP) is chosen as the precursor due to its relatively low dehalogenative reaction barrier.[13, 36] As illustrated in Figure 1a, upon adsorption of HBTP molecules on Ag(111), debromination can occur below room temperature, facilitated by the Ag adatoms to form organometallic intermediates. Subsequent annealing at temperatures ranging from 420 – 560 K leads to final [2+2] cycloaddition products after removing the Ag adatoms from the intermediates. In contrast, an extraordinary [2+2+2+2] cycloaddition reaction (Figure 1b) is identified on graphite by low-temperature scanning tunneling microscopy (STM), catalyzed by Fe guest atoms[37-39]via cross dehalogenative and dehydrogenative reactions. The reactions further demonstrate a domino-like fashion among homo-species to form one-dimensional (1D) grain boundaries (GBs), which are facilitated by the side-by-side intermolecular coupling and steric hindrance. Possible reaction pathways supported by density functional theoretical (DFT) calculations, indicate that the Fe atoms could play significant roles in anchoring the intermediates and products. This study offers new insights into the metal-mediated on-surface synthesis on inert substrates, which presents a promising route to fabricate diverse carbon-based nanostructures.

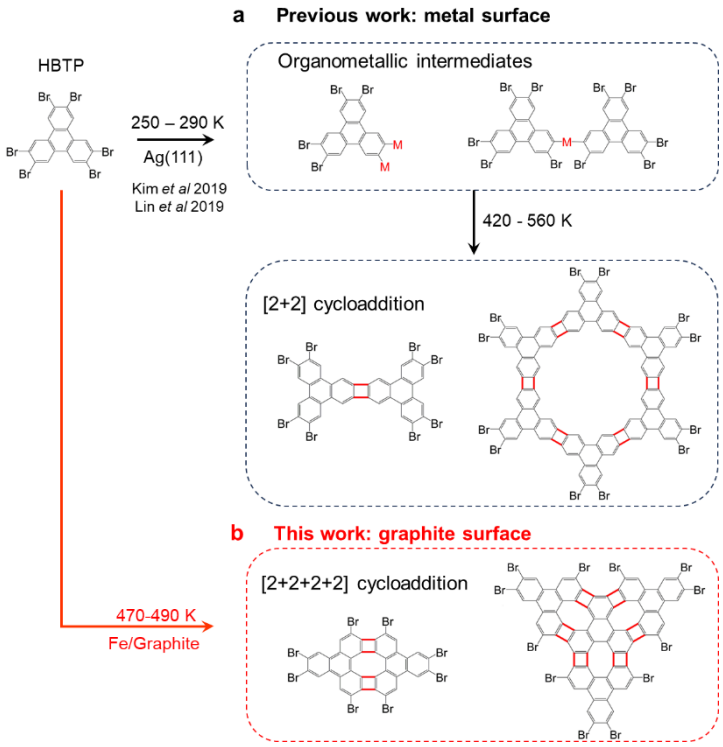

Figure 1. Cycloaddition reactions of HBTP molecules on different substrates. (a) Stepwise [2+2] cycloaddition reactions previously reported on Ag(111) with the presence of various organometallic intermediates [from Ref. 13, 36]. (b) [2+2+2+2] cycloaddition reactions assisted by Fe catalytic agent via cross dehalogenative and dehydrogenative reactions on graphite in this work.

Results and Discussion

Figure 2a demonstrates a STM image of the self-assembled HBTP monolayer on graphite surface (Experimental methods in supporting information, SI). Highly ordered, close-packed supramolecular arrays are formed with domain sizes extending over hundreds of nanometers. Upon closer inspection in Figure 2b, each HBTP molecule is discernible as a trefoil feature. It is found that under positive tip voltages (V_{tip}), the occupied states of the HBTP molecules located at its three peripheral aromatic rings (Figure S1). The unit cell is highlighted by a red rhombus, with experimental lattice constants of a = b = 1.24 ± 0.02 nm and γ = 59° ± 2°. These values are consistent with the DFT calculations optimized supramolecular structure on graphite as shown in Figure 2c, where a = b = 1.23 nm and γ = 60° (see DFT calculations of the unit cell in SI). The intermolecular Br-Br distance is 3.60 Å, aligning with previously reported values.[40, 41] This HBTP supramolecular array is mainly stabilized via the molecule-substrate π-π coupling and intermolecular halogen bonding. Furthermore, it is worth

noting that the assembly of achiral molecules on surfaces can induce chirality.[42, 43] The right (R) configuration is depicted in Figure 2c, and evidenced by Figure 2b and 2d. Examples of the left (L) configuration can be found in Figure 2e and Figure S4.

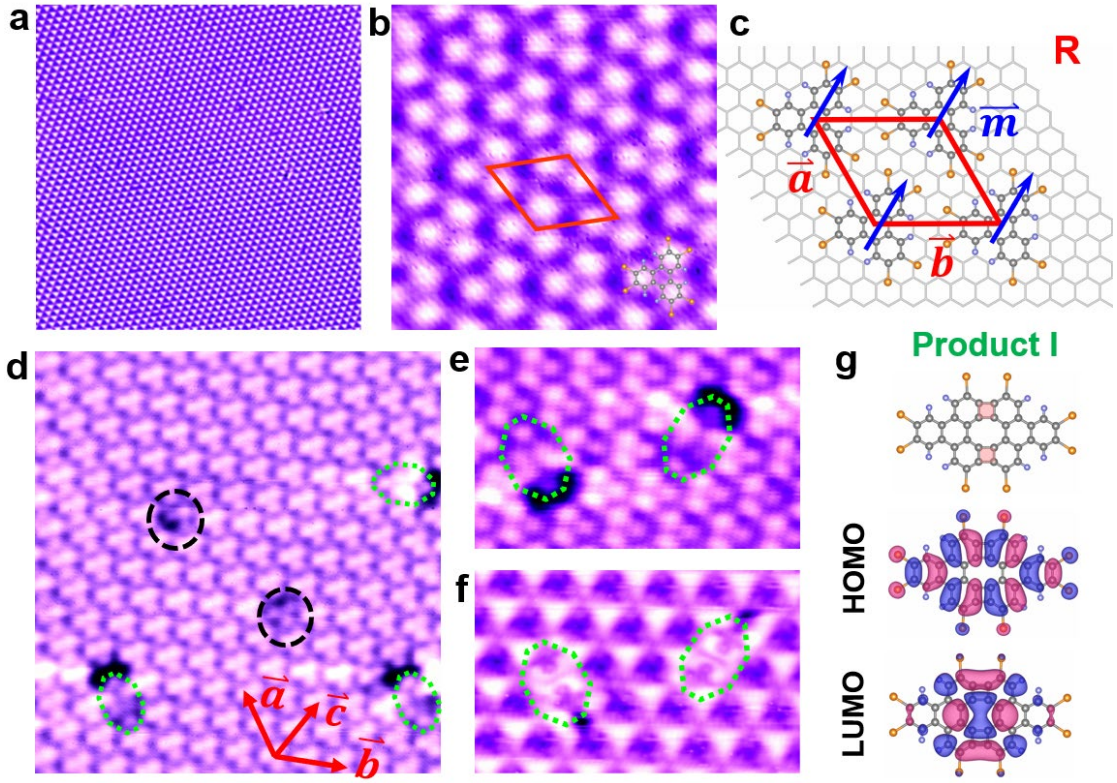

Figure 2. [2+2+2+2] cycloaddition reactions occurred in the highly-ordered HBTP supramolecular arrays. (a) Large-scale STM image of the highly-ordered, close-packed HBTP monolayer on graphite surface (50×50 nm^2; V_{tip} = -2.5 V, I = 40 pA). (b) Zoom-in topographic image revealing the trefoil feature of each HBTP molecule (5×5 nm^2; V_{tip} = 3.0 V, I = 30 pA). (c) The DFT optimized HBTP unit cell with right configuration on graphite. (d) Various 'defective' molecules are observable in the HBTP supramolecular arrays after dosing a few Fe atoms and annealing at 210°C (15×15 nm^2; V_{tip} = 3.0 V, I = 40 pA). (e) Occupied state of the product **I** (green polygons) formed by [2+2+2+2] cycloaddition recorded at V_{tip} = 3.4 V, and **f**, unoccupied state recorded at V_{tip} = -2.5 V, respectively (e and f, 8×5 nm^2; I = 80 pA). (g) Optimized structural model of the product **I**, and the corresponding HOMO and LUMO states (isoface = 0.01 e Å^{-3}). In panel (c) and (g), C atoms in the HBTP molecule and graphite are in dark and light grey, respectively; H and Br atoms are in cyan and gold, respectively.

Subsequently, Fe atoms were thermally evaporated onto the HBTP monolayer to trigger possible dehalogenative cycloaddition reactions (Experimental methods and Figure S5-S7 in SI). When a little amounts of Fe atoms (~0.01 ML) were dosed onto the HBTP arrays holding at 210°C, many defective molecules are observable in Figure 2d. They can be divided into two categories. The first species are highlighted by black

dashed circles, which retain the trefoil shapes with dim contrast. These are likely to be partially debrominated HBTP molecules, which had been previously reported on metal substrates.[13, 36] Such molecules can also be found in the as-grown HBTP monolayer after annealing at 200℃ without Fe catalyst (Figure S5).

The second species (product **I**) appear as spindle-like shapes, as highlighted by green polygons in Figure 2d, which can be easily distinguished from the surrounding HBTP molecules by its two-fold symmetry. Obviously, it is completely different from the [2+2] cycloaddition products with dog-bone-shapes on metal substrates.[13, 36] Here, the highly ordered HBTP supramolecular array is well preserved with the embedded product **I**, whose long axis is parallel to the $\vec{a}$, $\vec{b}$, and $\vec{c}$ orientations of the molecular arrays. Figure 2e and 2f represent the occupied and unoccupied states of this new species recorded at V_{tip} = 3.4 eV and V_{tip} = -2.5 eV, respectively. The possible supramolecular structure of the product **I** could be deduced by superimposing the benzenoid backbones of the HBTP molecules onto the molecularly resolved STM images (Figure S7). The proposed molecular model is depicted in Figure 2g, formed by two HBTP molecules fused together via complicated dehydrohalogenations following by side-by-side [2+2+2+2] cycloadditions. The calculated highest occupied molecular orbital (HOMO) and lowest unoccupied molecular orbital (LUMO) of the proposed model are in good agreement with the observed occupied (Figure 2e) and unoccupied states (Figure 2f) captured in STM images. The possible reasons for the absence of the head-to-head [2+2] cycloaddition (Figure 1a) will be discussed later. Many other possible products were also proposed for comparison in Figure S1-S3.

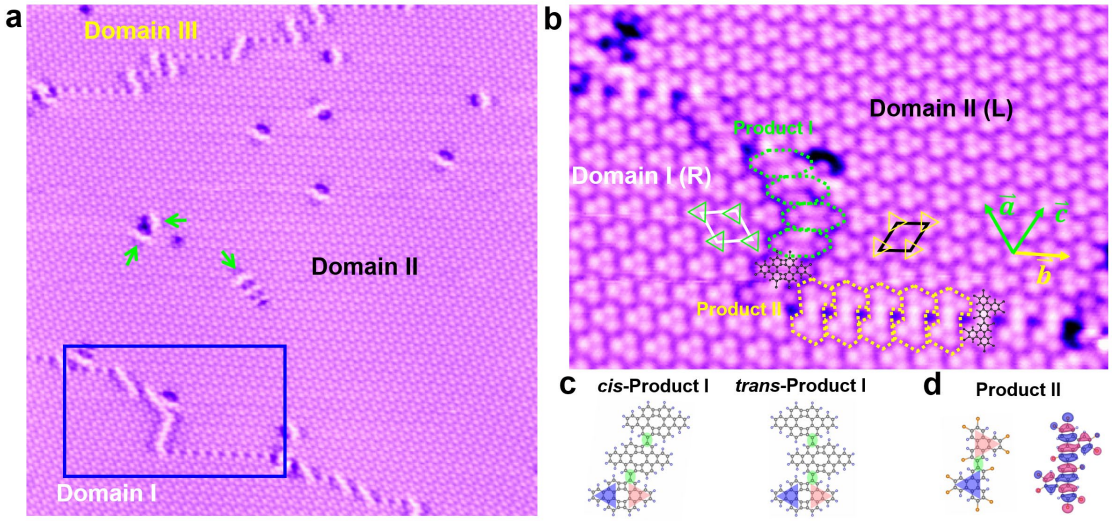

Figure 3. 1D GB constructed by 'defective' molecules. (a) Multiple domains with different molecular orientations are observed with the formation of 1D GBs (50×50 nm^2; V_{tip} = 3.0 V, I = 40 pA). The green arrows indicate three product **I** individuals along different orientations. (b) Enlarged STM image revealed that the GBs are composed by product **I** and **II** along $\vec{a}/\vec{c}$ and $\vec{b}$, respectively (14×20 nm^2; V_{tip} = 3.4 V, I = 50 pA). The black benzenoid backbones of the product **I** and **II** are superimposed for guiding eyes. (c) The schematic models of cis-product **I** and trans-product **I**. (d) Optimized structural model and calculated HOMO of product **II**. The green shadows highlight the intermolecular dehalogenations.

More dehalogenative products were obtained by increasing the Fe doses to ~0.1ML (Figure 3). Interestingly, 1D GBs constructed by defective-like molecules are observed in Figure 3a. Meanwhile, individual products **I** randomly distributed within the molecular domains are found, as indicated by the green arrows. Figure 3b represents a close-up of the GBs, enlarged from the region highlighted by a blue rectangle in Figure 3a. The unit cells of domain I and II are marked by white and black rhombuses, respectively, revealing the chirality induced upon adsorption. The GBs are formed along the highest symmetric orientations of the molecular array, i.e., $\vec{a}$, $\vec{b}$, and $\vec{c}$, with intersection angles of 60°. Interestingly, the basic building blocks of the GBs along $\vec{b}$ ($GB_{\vec{b}}$) are distinctly different from the other two along $\vec{a}$ ($GB_{\vec{a}}$) and $\vec{c}$ ($GB_{\vec{c}}$). In the $GB_{\vec{a}}$ and $GB_{\vec{c}}$, the building units highlighted by green spindle-like shapes are similar to product **I**. In fact, GBs along $\vec{a}$ and $\vec{c}$ are both constructed by 1D *cis*-product **I** chains via intermolecular C-C coupling, after debrominations at the sites denoted by green shadow in Figure 3c. Meanwhile, *trans*-product **I** emerges at the intersection of the $GB_{\vec{a}}$ and $GB_{\vec{c}}$ (Figure S8a). In contrast, the building block of $GB_{\vec{b}}$ is identified to be product

II with a dumbbell-shape, formed by a pair of debrominated HBTP molecules as shown in Figure 3d (Figure S3a). The benzenoid backbones of the product **I** and **II** are superimposed in Figure 3b for guiding eyes.

The formation of such 1D GBs suggest that the dehalogenative and dehydrogenative C-C coupling can occur in a domino-like fashion,[20] and the steric hindrance effect could play significant roles. It can be seen that the neighboring HBTP molecules across the $GB_{\vec{a}}$ and $GB_{\vec{c}}$ are packing in a side-to-side manner (Figure S4), thus facilitating the [2+2+2+2] cycloaddition reactions to form products **I**. While across the $GB_{\vec{b}}$, the neighboring molecules are aligned in a head-to-head manner (Figure S4) to form products **II**. In fact, the irregular GBs are mixtures of products **I** along $GB_{\vec{a}}$/$GB_{\vec{c}}$ and products **II** along $GB_{\vec{b}}$ (Figure S8a). The length of the regular $GB_{\vec{a}}$ or $GB_{\vec{c}}$ composed by cis-product **I** can extend over tens of nanometers, e.g., ~30 nm (Figure S8b). The GBs divide the large, homogeneous domains with single packing configuration into small, heterogeneous domains with mirror-symmetric configurations.

Close-packed supramolecular islands extending over 100 nm persist on the graphite surface even with more than 30% products (Figure S9). As shown in Figure 4a, when the total products reach ~30%, HBTP molecular domains decrease to several nanometers only, and larger supramolecules or even polymers based on the product **I** and **II** are formed. For instance, Figure 4b demonstrates a trimer **I** formed by dibrominated C-C coupling (highlighted by red bonds) of three HBTP molecules, derived from product **II**; while Figure 4c and 4d show a trimer **II** and a tetramer respectively, derived from product **I** via multiple dehydrohalogenations and [2+2+2+2] cycloadditions (red bonds). Furthermore, trimer **I** and **II** can be considered as new types of GBs, where the molecules in the upper and bottom domains separated by these trimers possess the same orientation. More examples are given in Figure S9.

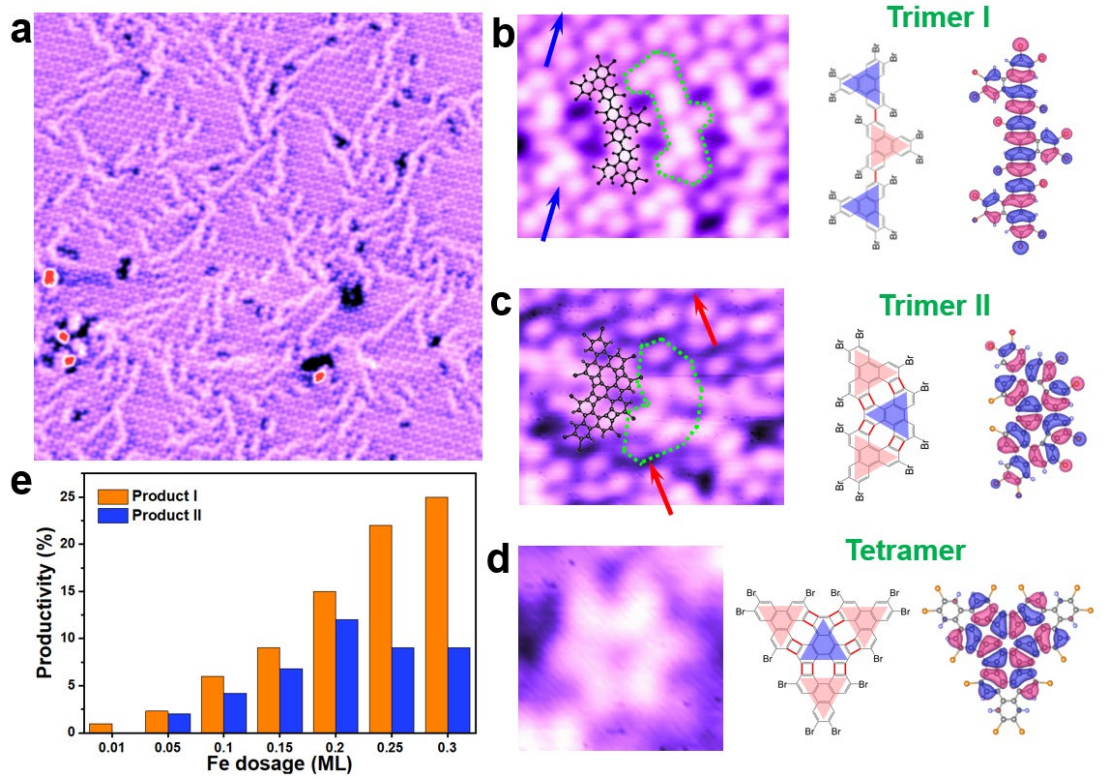

Figure 4. Products at high Fe dosage (~0.3 ML). (a) The formation of close-packed molecular domains with a high density of reaction products and dendritic GBs (50×50 nm^2; V_{tip} = 3.0 V, I = 10 pA). (b-d) Left: STM images of trimer **I** (b), trimer **II** (c), and tetramer (d) (b, 5.5×4.5 nm^2; V_{tip} = 3.0 V, I = 80 pA; c, 5.4×4.4 nm^2; V_{tip} = 3.0 V, I = 20 pA; d, 2.7×2.7 nm^2; V_{tip} = 2.6 V, I = 10 pA). Middle: the corresponding molecular models. Right: the corresponding HOMO states (Figure S3). (e) Statistical productivities of product **I** and **II** with the increasing Fe dosages. Each dosage was statistically analyzed over thousands of molecules.

Consequently, we analyze the productivities of product **I** and **II** under various Fe dosages in Figure 4e, which quantitatively increase with the Fe dosages. Products **I** can be obtained as individuals at extremely low Fe dosage (e.g., ~0.01 ML) (Figure 2), while products **II** are found at GBs as the dosage increases to ~0.05 ML and above (Figure 3). Overall, the product **I** (golden column) increases faster and dominates over the product **II**, and its productivity can reach as high as ~25% within the investigated range. In contrast, the productivity of product **II** (blue column) reaches its maximum at ~12% with ~0.2 ML Fe, and almost saturate at ~10% with even higher Fe dosages. This phenomenon seems anomalous, as the formation of product **I** involves much complicated multiple debromination, dehydrogenation and recombination processes, while product **II** only requires a bi-debromination and a C-C bonding reaction. The underlying mechanisms are explored in below.

To understand the formation processes of product **I** on the graphite substrate, we divided the reactions into five possible steps: 0) Fe-assisted debromination; 1) the 1st

dehydrogenation; 2) the 2nd dehydrogenation; 3) desorption of two HBr molecules; and 4) [2+2+2+2] cycloaddition. Firstly, DFT calculation results suggest that the step 0), debromination, is exothermic (Figure S10). This implies that debromination could occur spontaneously upon capturing Fe atoms near the HBTP molecule. Additionally, it is found that the single HBPT molecule interacts weakly with graphite via van der Waals forces, while the Fe atoms anchor the HBPT on the surface, thus facilitating the subsequent reactions. In the following step 1), the initial configuration 0 is formed by two Fe atoms bridging the debrominated HBTP (debr-HBTP) molecule and the Br atoms (Figure 5c), due to the spontaneous breakage of the C-Br bonds. Then one C-H bond next to the debromination site is activated and broken, forming an HBr molecule adsorbed nearby the Fe atom (configuration 5 in Figure 5c). This process repeats again in the step 2) to form the 2nd HBr molecule (Figure 5d). Figure 5a reveals that the energy barrier for the 1st dehydrogenation (configuration 0-5) is 1.23 eV (Δ_1), which slightly increases to 1.42 eV (Δ_2) for the 2nd one (configuration 5-10) due to the positively charged HBTP molecule. After these two steps, the debrominated and dehydrogenated HBTP (debr-dehy-HBTP) molecule is still anchored on the graphite surface via the Fe atoms, and the two HBr molecules are physisorbed, as demonstrated in configuration 10, Figure 5d. In the step 3). Then, these two HBr molecules diffuse away from the reaction sites (Figure 5e) via a small energy barrier of 0.68 eV (Δ_3), which indicates the possibility of releasing at even room temperature (a barrier of ~30 $k_B T$, $\approx$ 0.77 eV). In the final step 4), two debr-dehy-HBTP molecules are placed side-to-side for the [2+2+2+2] cycloaddition (configuration 0 in Figure 5f). These two molecules could spontaneously slide closer to each other (configuration 0 to 3 in Figure 5f), which is exothermic as revealed by Figure 5b. Then the recombination of the first pair of C-C bonds (configuration 3 to 4 in Figure 5f), namely the first half of the [2+2+2+2] cycloaddition, is endothermic with an energy barrier of 0.72 eV (Δ_4), while the second half of the [2+2+2+2] cycloaddition (configuration 4 to 6 in Figure 5f) is exothermic.

According to this proposed step-by-step reaction pathway for the product **I**, the highest energy barrier to be overcome is the 2nd dehydrogenation, namely Δ_2 = 1.42 eV, which is possible upon mild annealing at ~210°C. Indeed, this temperature is relatively low compared to that usually required to active dehydrogenation and/or eliminate organometallic intermediates on metal substrates.[10, 22, 36, 44, 45] Furthermore, the side-views of all these configurations discussed in Figure 5c-f are shown in Figure S11. It is

worth noting that the Fe atoms are intercalating between the intermediates/products and the graphite substrate to increase the stability. In particular, after the [2+2+2+2] cycloaddition reactions, the Fe atoms are sandwiched between product **I** and graphite as shown in Figure 5f and Figure S11d. Further MD calculations demonstrates that the Fe atoms could escape within 5 ps at 600 K (Figure S12). In fact, many $FeBr_x$ clusters and domains are observable at the edges of the molecular islands after annealing (e.g., Figure S6e and Figure S8b).

We also calculated the possible reaction pathways of the product **II** (Figure S13). The formation requires breaking two C-Br bonds in a pair of HBTP molecules, and subsequently recombining them via a C-C coupling. The energy barriers are relatively low, only 0.83 eV and 0.58 eV, respectively. Usually, the productivities depend on the activation energies, the lower the energy barrier, the higher the productivity. Thus, it is unusual that the products **I** are always more than the products **II**. One possible reason is the steric hindrance effect. The products **II** only exist in the 1D GBs, but no individual is found inside the molecular domains. Furthermore, the product **I** could be held by two de-Br-HBTP molecules at the sides via chemical coupling, namely product **I'** shown in Figure S1c and Figure S7. Such intermolecular coupling might not only enhance its stability on the graphite surface, but also reduce the reaction barrier to form product **I'**.

Finally, possible pathways lead to the head-to-head [2+2] cycloaddition reactions (Figure 1a) were considered, which are distinguishing from that on Ag(111).[36] As shown in Figure S14, the formation of the [2+2] cycloaddition product involves two debrominations and two C-C bonding processes without dehydrogenation. However, the energy barriers for the 1st and 2nd C-C coupling in the [2+2] cycloaddition are as high as 3.05 eV and 1.94 eV, respectively. These barriers are much higher than that for the product **I**, making its absence reasonable. Such phenomena are distinct from those on intensively studied metal surface, where individual intermediates/products could strongly interact with the substrates. In the supramolecular array assembled on graphite, the steric hindrance effect and intermolecular coupling become significant and could redirect the reaction pathways.

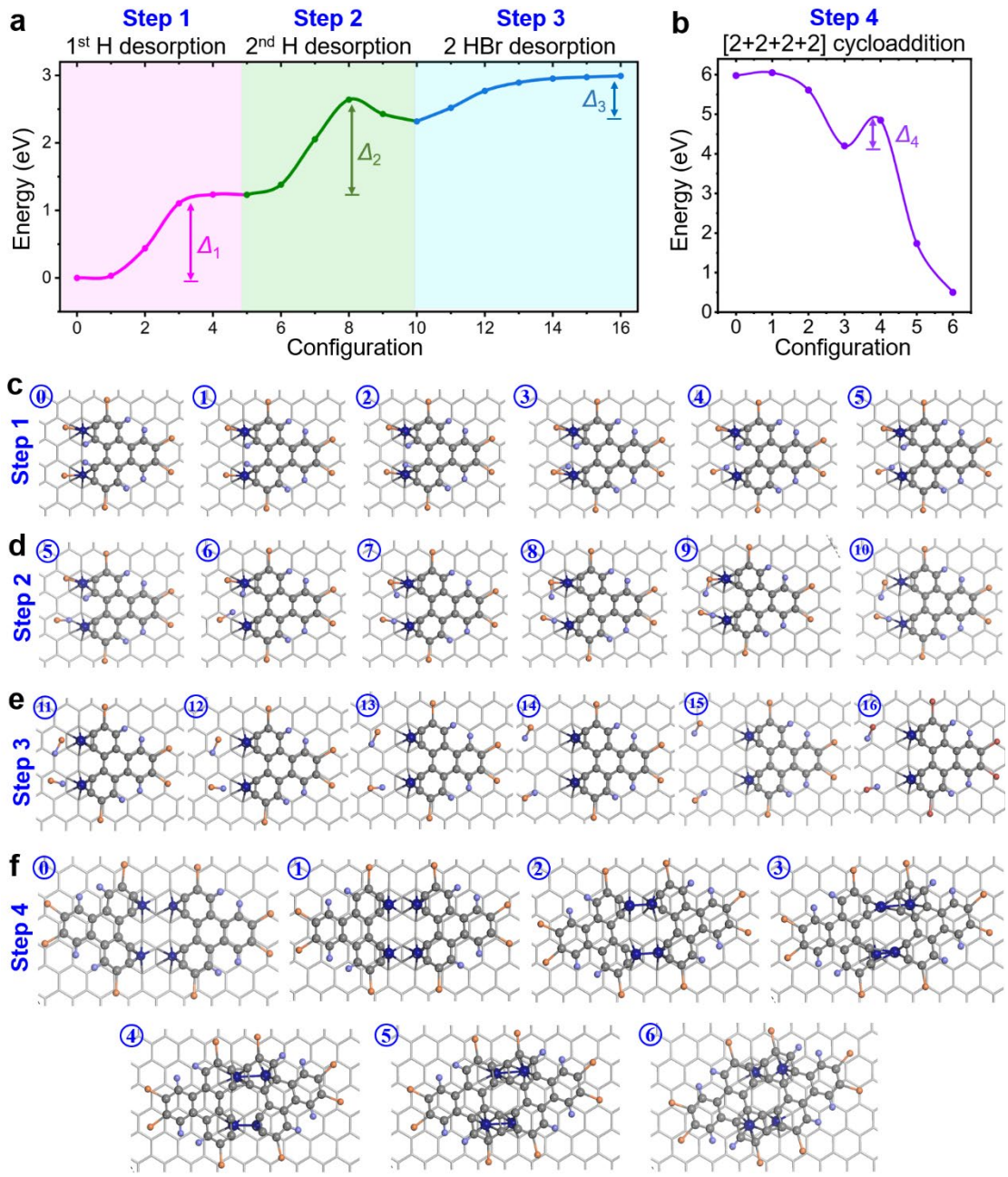

Figure 5. Possible reaction pathways of the product **I**. (a) The energy profile of the dehydrogenations of the 1st (step 1) and 2nd (step 2) H atoms, and the desorption of the two HBr molecules (step 3) for a single HBTP molecule. (b) The energy diagram of the [2+2+2+2] cycloaddition of two debr-dehy-HBTP molecules (step 4). (c-f) The corresponding configurations of the possible transition states with local energetic minima of the step 1-4 in the panel (a) and (b). C atoms in the HBTP molecule and graphite are in dark and light grey, respectively; H, Br and Fe atoms are in cyan, gold and blue, respectively.

In conclusion, we have demonstrated the redirected on-surface synthesis on the chemically inert graphite surface, where [2+2+2+2] cycloaddition reactions are observed in the self-assembled HBTP molecular arrays via Fe-catalyzed dehydrohalogenations. Various products are observed as the dosage of Fe catalytic

agents increases, including product **I**, product **II**, and their derivates. Additionally, DFT calculations were conducted to explore the possible reaction pathways of the products **I** and **II**, as well as the excluded [2+2] cycloadditions. It suggests that the Fe catalysts anchor the organic intermediates/products on the graphite surface to facilitate the reactions, in whichthe formation of the major product **I** via [2+2+2+2] cycloaddition could be promoted by additional intermolecular coupling and steric hindrance effect. These findings reveal the emergence of entirely different products and a distinct reaction mechanism on graphite. This study could promote further studies of the on-surface synthesis on weakly interacting substrates, opening a new access to engineer carbon-based nanostructures.

Competing interests

The authors declare no competing interests.

Acknowledgements

Y.L.H. acknowledges financial support from the National Natural Science Foundation of China (Grant No.12350610236) and the Natural Science Foundation of Fujian Province (2022J06035). M. Y. acknowledges the funding support from the Hong Kong Polytechnic University (project numbers.: P0034827, P0042711, P0039734, and P0039679), PolyU RCNN (Project No.: P0048122), Department of Science and Technology of Guangdong Province (GDSTC) (Project No.: P0046476), and Research Grants Council, Hong Kong (project number: 25301523). J.Y. and Y.-W.Z. acknowledge the supports by Italy-Singapore Science and Technology Cooperation (Grant No. R23101R040), and Singapore A*STAR SERC CRF Award, and the computing resources at the A*STAR Computational Resource Centre and National Supercomputer Centre, Singapore. A.T.S.W acknowledges the support of the National Research Foundation of Singapore CRP26-2021RS-0001.

Reference

(1) Grill, L.; Hecht, S. Covalent on-surface polymerization. *Nat. Chem.* **2020**, *12*, 115-130.

(2) Houtsma, R. S. K.; de la Rie, J.; Stohr, M. Atomically precise graphene nanoribbons: interplay of structural and electronic properties. *Chem. Soc. Rev.* **2021**, *50*, 6541-6568.

(3) Clair, S.; de Oteyza, D. G. Controlling a Chemical Coupling Reaction on a Surface: Tools and Strategies for On-Surface Synthesis. *Chem. Rev.* **2019**, *119*, 4717-4776.

(4) Treier, M.; Pignedoli, C. A.; Laino, T.; Rieger, R.; Mullen, K.; Passerone, D.; Fasel, R. Surface-assisted cyclodehydrogenation provides a synthetic route towards easily processable and chemically tailored nanographenes. *Nat. Chem.* **2011**, *3*, 61-67.

(5) Mishra, S.; Catarina, G.; Wu, F.; Ortiz, R.; Jacob, D.; Eimre, K.; Ma, J.; Pignedoli, C. A.; Feng, X.; Ruffieux, P.; et al. Observation of fractional edge excitations in nanographene spin chains. *Nature* **2021**, *598*, 287-292.

(6) Sanchez-Sanchez, C.; Nicolai, A.; Rossel, F.; Cai, J.; Liu, J.; Feng, X.; Mullen, K.; Ruffieux, P.; Fasel, R.; Meunier, V. On-Surface Cyclization of ortho-Dihalotetracenes to Four- and Six-Membered Rings. *J. Am. Chem. Soc.* **2017**, *139*, 17617-17623.

(7) Huang, H.; Wei, D.; Sun, J.; Wong, S. L.; Feng, Y. P.; Neto, A. H.; Wee, A. T. Spatially resolved electronic structures of atomically precise armchair graphene nanoribbons. *Sci. Rep.* **2012**, *2*, 983.

(8) Zhou, X.; Yu, G. Modified Engineering of Graphene Nanoribbons Prepared via On-Surface Synthesis. *Adv. Mater.* **2020**, *32*, e1905957.

(9) Tran, B. V.; Pham, T. A.; Grunst, M.; Kivala, M.; Stohr, M. Surface-confined [2 + 2] cycloaddition towards one-dimensional polymers featuring cyclobutadiene units. *Nanoscale* **2017**, *9*, 18305-18310.

(10) Zint, S.; Ebeling, D.; Schloder, T.; Ahles, S.; Mollenhauer, D.; Wegner, H. A.; Schirmeisen, A. Imaging Successive Intermediate States of the On-Surface Ullmann Reaction on Cu(111): Role of the Metal Coordination. *ACS Nano* **2017**, *11*, 4183-4190.

(11) Björk, J.; Hanke, F.; Stafström, S. Mechanisms of Halogen-Based Covalent Self-Assembly on Metal Surfaces. *J. Am. Chem. Soc.* **2013**, *135*, 5768-5775.

(12) Bieri, M.; Nguyen, M.-T.; Groning, O.; Cai, J.; Treier, M.; Ait-Mansour, K.; Ruffieux, P.; Pignedoli, C. A.; Passerone, D.; Kastler, M.; et al. Two-Dimensional Polymer Formation on Surfaces: Insight into the Roles of Precursor Mobility and Reactivity. *J. Am. Chem. Soc* .**2010**, *132*, 16669-16676.

(13) Zhang, R.; Xia, B.; Xu, H.; Lin, N. Identifying Multinuclear Organometallic Intermediates in On-Surface [2+2] Cycloaddition Reactions. *Angew. Chem. Int. Ed. Engl.* **2019**, *58*, 16485-16489.

(14) Lyu, B.; Chen, J.; Lou, S.; Li, C.; Qiu, L.; Ouyang, W.; Xie, J.; Mitchell, I.; Wu, T.; Deng, A.; et al. Catalytic Growth of Ultralong Graphene Nanoribbons on Insulating Substrates. *Adv. Mater.* **2022**, e2200956.

(15) Blackwell, R. E.; Zhao, F.; Brooks, E.; Zhu, J.; Piskun, I.; Wang, S.; Delgado, A.; Lee, Y. L.; Louie, S. G.; Fischer, F. R. Spin splitting of dopant edge state in magnetic zigzag graphene nanoribbons. *Nature* **2021**, *600*, 647-652.

(16) Jacobse, P. H.; Mangnus, M. J. J.; Zevenhuizen, S. J. M.; Swart, I. Mapping the Conductance of Electronically Decoupled Graphene Nanoribbons. *ACS Nano* **2018**, *12*, 7048-7056.

(17) Sun, K.; Fang, Y.; Chi, L. On-Surface Synthesis on Nonmetallic Substrates. *ACS Mater. Lett.* **2020**, *3*, 56-63.

(18) Jiang, S.; Neuman, T.; Boeglin, A.; Scheurer, F.; Schull, G. Topologically localized excitons in single

graphene nanoribbons. *Science* **2023**, *379*, 1049–1053.
(19) Lackinger, M. Synthesis on inert surfaces. *Dalton Trans* **2021**, *50*, 10020-10027.
(20) Ma, C.; Wang, J.; Ma, H.; Yin, R.; Zhao, X. J.; Du, H.; Meng, X.; Ke, Y.; Hu, W.; Li, B.; et al. Remote-Triggered Domino-like Cyclodehydrogenation in Second-Layer Topological Graphene Nanoribbons. *J. Am. Chem. Soc.* **2023**, *145*, 10126-10135.
(21) Lyu, B.; Chen, J.; Wang, S.; Lou, S.; Shen, P.; Xie, J.; Qiu, L.; Mitchell, I.; Li, C.; Hu, C.; *et al.* Graphene nanoribbons grown in hBN stacks for high-performance electronics. *Nature* **2024**, *628*, 758-764.
(22) Kolmer, M.; Zuzak, R.; Steiner, A. K.; Zajac, L.; Engelund, M.; Godlewski, S.; Szymonski, M.; Amsharov, K. Fluorine-programmed nanozipping to tailored nanographenes on rutile TiO2 surfaces. *Science* **2019**, *363*, 57-60.
(23) Kolmer, M.; Steiner, A.-K.; Izydorczyk, I.; Ko, W.; Engelund, M.; Szymonski, M.; Li, A.-P.; Amsharov, K. Rational synthesis of atomically precise graphene nanoribbons directly on metal oxide surfaces. *Science* **2020**, *369*, 571–575.
(24) Richter, A.; Haapasilta, V.; Venturini, C.; Bechstein, R.; Gourdon, A.; Foster, A. S.; Kuhnle, A. Diacetylene polymerization on a bulk insulator surface. *Phys. Chem. Chem. Phys.* **2017**, *19*, 15172-15176.
(25) Palma, C. A.; Diller, K.; Berger, R.; Welle, A.; Bjork, J.; Cabellos, J. L.; Mowbray, D. J.; Papageorgiou, A. C.; Ivleva, N. P.; Matich, S.; et al. Photoinduced C-C reactions on insulators toward photolithography of graphene nanoarchitectures. *J. Am. Chem. Soc.* **2014**, *136*, 4651-4658.
(26) Fatayer, S.; Moll, N.; Collazos, S.; Perez, D.; Guitian, E.; Pena, D.; Gross, L.; Meyer, G. Controlled Fragmentation of Single Molecules with Atomic Force Microscopy by Employing Doubly Charged States. *Phys. Rev. Lett.* **2018**, *121*, 226101.
(27) Sun, L.; Zheng, W.; Gao, W.; Kang, F.; Zhao, M.; Xu, W. On-surface synthesis of aromatic cyclo[10]carbon and cyclo[14]carbon. *Nature* **2023**, *623*, 972-976.
(28) Yu, M.; Chen, C.; Liu, Q.; Mattioli, C.; Sang, H.; Shi, G.; Huang, W.; Shen, K.; Li, Z.; Ding, P.; et al. Long-range ordered and atomic-scale control of graphene hybridization by photocycloaddition. *Nat. Chem.* **2020**, *12*, 1035-1041.
(29) Zhao, W.; Dong, L.; Huang, C.; Win, Z. M.; Lin, N. Cu- and Pd-catalyzed Ullmann reaction on a hexagonal boron nitride layer. *Chem. Commun.* **2016**, *52*, 13225-13228.
(30) Summerfield, A.; Baldoni, M.; Kondratuk, D. V.; Anderson, H. L.; Whitelam, S.; Garrahan, J. P.; Besley, E.; Beton, P. H. Ordering, flexibility and frustration in arrays of porphyrin nanorings. *Nat. Commun.* **2019**, *10*, 2932.
(31) Zhan, G.; Cai, Z. F.; Strutynski, K.; Yu, L.; Herrmann, N.; Martinez-Abadia, M.; Melle-Franco, M.; Mateo-Alonso, A.; Feyter, S. Observing polymerization in 2D dynamic covalent polymers. *Nature* **2022**, *603*, 835-840.
(32) Daelemans, B.; Bilbao, N.; Dehaen, W.; De Feyter, S. Carbocatalysis with pristine graphite: on-surface nanochemistry assists solution-based catalysis. *Chem. Soc. Rev.* **2021**, *50* , 2280-2296.
(33) Fabozzi, F. G.; Severin, N.; Rabe, J. P.; Hecht, S. Room Temperature On-Surface Synthesis of a Vinylene-Linked Single Layer Covalent Organic Framework. *J. Am. Chem. Soc.* **2023**, *145*, 18205-18209.
(34) Niu, W.; Fu, Y.; Serra, G.; Liu, K.; Droste, J.; Lee, Y.; Ling, Z.; Xu, F.; Cojal González, J. D.; Lucotti, A.; *et al*. Bottom-up Solution Synthesis of Graphene Nanoribbons with Precisely Engineered Nanopores. *Angew. Chem. Inter. Ed.* **2023**, *62*, e202305737.
(35) Grossmann, L.; King, B. T.; Reichlmaier, S.; Hartmann, N.; Rosen, J.; Heckl, W. M.; Bjork, J.; Lackinger, M. On-surface photopolymerization of two-dimensional polymers ordered on the mesoscale.

Nat. Chem. **2021**, *13*, 730-736.
(36) Zhang, C.; Kazuma, E.; Kim, Y. Atomic-Scale Visualization of the Stepwise Metal-Mediated Dehalogenative Cycloaddition Reaction Pathways: Competition between Radicals and Organometallic Intermediates. *Angew. Chem. Int. Ed. Engl.* **2019**, *58*, 17736-17744.
(37) Lin, T.; Shang, X. S.; Adisoejoso, J.; Liu, P. N.; Lin, N. Steering on-surface polymerization with metal-directed template. *J. Am. Chem. Soc.* **2013**, *135*, 3576-3582.
(38) Xing, S.; Zhang, Z.; Fei, X.; Zhao, W.; Zhang, R.; Lin, T.; Zhao, D.; Ju, H.; Xu, H.; Fan, J.; et al. Selective on-surface covalent coupling based on metal-organic coordination template. *Nat. Commun.* **2019**, *10*, 70.
(39) Xue, Q.; Xue, N.; Li, J.; Li, Y.; Li, R.; Zhang, Y.; Li, N.; Shen, Z.; Hou, S.; Wang, Y. Self-Assembly of a Metal–Organic Framework by Stepwise Coordination of Carboxyl and Pyrrolyl Groups. *J. Phys. Chem. C* **2020**, *124*, 7790-7796.
(40) Song, W.; Martsinovich, N.; Heckl, W. M.; Lackinger, M. Thermodynamics of halogen bonded monolayer self-assembly at the liquid-solid interface. *Chem. Commun.* **2014**, *50*, 13465-13468.
(41) Han, Z.; Czap, G.; Chiang, C.-l.; Xu, C.; Wagner, P. J.; Wei, X.; Zhang, Y.; Wu, R.; Ho, W. Imaging the halogen bond in self-assembly halogenbenzenes on silver. *Science* **2017**, *358*, 206-210.
(42) Ernst, K. H. Molecular chirality at surfaces. *Phys. Status Solidi B* **2012**, *249*, 2057-2088.
(43) Cai, L.; Gao, T.; Wee, A. T. S. Topology selectivity of a conformationally flexible precursor through selenium doping. *Nat. Commun.* **2024**, *15*, 3235.
(44) Zeng, Z.; Guo, D.; Wang, T.; Chen, Q.; Matej, A.; Huang, J.; Han, D.; Xu, Q.; Zhao, A.; Jelinek, P.; et al. Chemisorption-Induced Formation of Biphenylene Dimer on Ag(111). *J. Am. Chem. Soc.* **2022**, *144*, 723-732.
(45) Cai, J.; Ruffieux, P.; Jaafar, R.; Bieri, M.; Braun, T.; Blankenburg, S.; Muoth, M.; Seitsonen, A. P.; Saleh, M.; Feng, X.; *et al.* Atomically precise bottom-up fabrication of graphene nanoribbons. *Nature* **2010**, *466*, 470-473.

Table of Content

On-surface synthesis on chemically inert substrates via thermally activation is extremely challenging in ultra-high vacuum, suffering from a severe “desorption problem”. Here, we report an extraordinary side-to-side [2+2+2+2] cycloaddition via dehydrohalogenations in a highly ordered self-assembled molecular array on graphite, where the cycloaddition products are embedded as defective individuals or chains (grain boundaries) even with product density up to ~30%.